

Effects of Numerical Integration on DLM/FD Method for Solving Interface Problems with Body-Unfitted Meshes *

Cheng Wang¹, Pengtao Sun², Rihui Lan², Hao Shi¹, and Fei Xu³

¹ School of Mathematical Sciences, Tongji University, Shanghai, China
wangcheng@tongji.edu.cn (Cheng Wang), sh1009@163.com (Hao Shi)

² Department of Mathematical Sciences, University of Nevada, Las Vegas, Nevada
pengtao.sun@unlv.edu (Pengtao Sun), lanr1@unlv.nevada.edu (Rihui Lan)

³ Beijing Institute for Scientific and Engineering Computing, Beijing University of Technology, Beijing, China. xufei@lsec.cc.ac.cn

Abstract. In this paper, the effects of different numerical integration schemes on the distributed Lagrange multiplier/fictitious domain (DLM/FD) method with body-unfitted meshes are studied for solving different types of interface problems: elliptic-, Stokes- and Stokes/elliptic-interface problems. Commonly-used numerical integration schemes, compound type formulas and a specific subgrid integration scheme are presented for the mixed finite element approximation and the comparison between them is illustrated in numerical experiments, showing that different numerical integration schemes have significant effects on approximation errors of the DLM/FD finite element method for different types of interface problems, especially for Stokes- and Stokes/elliptic-interface problems, and that the subgrid integration scheme always results in numerical solutions with the best accuracy.

1 Introduction

Physical phenomena in a domain consisting of multiple materials and/or multi-phase fluids, which are immiscible and are divided by distinct interfaces, are often modeled by either identical or different partial differential equations with discontinuous coefficients on both sides of interfaces. These problems are generally called interface problems, sometimes called interaction problems in some specific scenarios such as fluid-structure interaction (FSI) problems, e.g., see [5, 17] and others references therein. In the past several decades, two major numerical approaches – the body-fitted mesh method and the body-unfitted mesh method – have been developed for tackling interface problems, which are classified by how the computational mesh and then the interface conditions are handled along the interface. In contrast to the body-fitted mesh method such as the arbitrary Lagrangian-Eulerian (ALE) method [8, 9], which is obliged to adapt the mesh to accommodate the motion of the interface, the body-unfitted mesh method, due to its simplicity in the mesh generation, becomes more promising and more advantageous for interface problems whose interfaces may bear a large deformation/displacement, such as the immersed boundary method (IBM) [12, 14], the

*Supported by NSF DMS-1418806 (Pengtao Sun) and NSFC-11801021 (Fei Xu)

distribute Lagrange multiplier/fictitious domain (DLM/FD) method [1, 7], the immersed finite element method (IFEM) [10, 11], and etc.

Among the aforementioned body-unfitted mesh methods, taking all properties of reliability, accuracy, flexibility and theoretical guarantees into consideration, the DLM/FD method has shown a lot of strengths and potentials in theoretical analyses as well as practical applications for general interface problems, and has gained considerable popularity in simulating FSI problems as well. So in this paper, we focus on the DLM/FD method, where a fictitious equation that is defined in one subdomain is introduced to cover the other subdomain, and its mesh is fixed in the entire domain as a background mesh and needs not to be updated even if the interface moves or deforms. Benefited from this feature, the DLM/FD method has become more popular in the simulation of FSI problems, especially in the case of an immersed structure with large deformation/displacements. To enforce the interface conditions, the DLM/FD method introduces the Lagrange multiplier (a pseudo body force) to weakly enforce the fictitious variables equal everywhere to the primary variables of the equation defined in the immersed domain and on the interface too. A monolithic system bearing a saddle-point structure is thus formed in regard to the Lagrange multiplier and primary variables. Therefore, the classical Babuška–Brezzi’s theory [4, 3] can be employed to prove the well-posedness, stability as well as convergence properties of the DLM/FD finite element method [2, 15].

To implement the DLM/FD method, an accurate and also efficient numerical integration scheme is needed to calculate the integration in which the distributed Lagrange multiplier is involved. For instance, (21) can be referred to in advance to preview the significance, where, in the finite element computation on each immersed element for the Lagrange multiplier terms denoted by the dual inner product $\langle \lambda, v_h|_{\Omega} \rangle_{\Omega_2}$, the integrand function is a product of two piecewise polynomials which are defined on two non-matched meshes, $T_h(\Omega)$ and $T_H(\Omega_2)$. Although the piecewise polynomial defined on $T_h(\Omega)$, $v_h|_{\Omega}$, can be transferred to $T_H(\Omega_2)$ through the interpolation approach, it is no longer sufficiently smooth in each immersed element of $T_H(\Omega_2)$ just because of the non-matching between $T_h(\Omega)$ and $T_H(\Omega_2)$. Thus we can not conclude that the commonly-used higher order numerical integration scheme will lead to a higher accuracy for those Lagrange multiplier terms.

The object of this paper is to study the effects of various numerical integration schemes on the performance of the DLM/FD methods for solving different interface problems with jump coefficients. Essentially, we do not want to let the accuracy of numerical integration influence the overall approximation accuracy, especially when the DLM/FD method is used for simulating complex problems, e.g., FSI problems. However, we find out different numerical integration methods indeed have significant effects on approximation errors of the DLM/FD method for different types of interface problems. Three types of numerical integration schemes are considered in our study: the commonly-used numerical integration schemes (see e.g. [6]), the compound type formulas, and the subgrid integration scheme proposed in [18]. Numerical results presented in Section 4 shows that the

performance of DLM/FD method for solving elliptic interface problems is insensitive to the numerical integration but is sensitive to Stokes- and Stokes/elliptic-interface problems, and that the subgrid integration scheme always leads to the approximation solution of the highest accuracy.

The rest of this paper is organized as follows. The DLM/FD finite element method for solving different types of interface problems are recalled in Section 2. Several commonly-used numerical integration schemes, the compound type formulas and the subgrid integration technique are introduced in Section 3. Numerical performances are shown in Section 4.

2 DLM/FD method for three types of interface problems

In this section, we briefly recall the DLM/FD finite element method for solving three different types of interface problems with jump coefficients.

2.1 Three types of interface problems

The first type is the elliptic interface problem, defined as

$$-\nabla \cdot (\beta_1 \nabla u_1) = f_1, \quad \text{in } \Omega_1, \quad (1)$$

$$-\nabla \cdot (\beta_2 \nabla u_2) = f_2, \quad \text{in } \Omega_2, \quad (2)$$

$$u_1 = u_2, \quad \text{on } \Gamma, \quad (3)$$

$$\beta_1 \nabla u_1 \cdot \mathbf{n}_1 + \beta_2 \nabla u_2 \cdot \mathbf{n}_2 = w, \quad \text{on } \Gamma, \quad (4)$$

$$u_1 = 0, u_2 = 0, \quad \text{on } \partial\Omega \setminus \Gamma, \quad (5)$$

where, $\Omega = \Omega_1 \cup \Omega_2 \subset \mathcal{R}^d$ (see Fig. 1), the interface $\Gamma = \partial\Omega_2$ is a closed curve that divides the domain Ω into an interior region Ω_2 and an exterior region Ω_1 , \mathbf{n}_1 and \mathbf{n}_2 stand for the unit outward normal vectors on $\partial\Omega_1$ and $\partial\Omega_2$, respectively. u , that is defined in Ω , satisfies $u|_{\Omega_1} = u_1$, $u|_{\Omega_2} = u_2$ which are associated with $f \in L^2(\Omega)$ and $f|_{\Omega_1} = f_1 \in L^2(\Omega_1)$, $f|_{\Omega_2} = f_2 \in L^2(\Omega_2)$. $\beta \in L^\infty(\Omega)$ satisfies $\beta|_{\Omega_1} = \beta_1 \in W^{1,\infty}(\Omega_1)$, $\beta|_{\Omega_2} = \beta_2 \in W^{1,\infty}(\Omega_2)$ and $\beta_1 \neq \beta_2$.

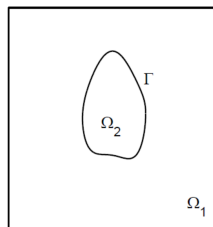


Fig. 1. Graphical depiction of the domain with an immersed interface.

The second type is the Stokes interface problem, defined as

$$-\nabla \cdot (\beta_1 \nabla \mathbf{u}_1) + \nabla p_1 = \mathbf{f}_1, \quad \text{in } \Omega_1, \quad (6)$$

$$\nabla \cdot \mathbf{u}_1 = 0, \quad \text{in } \Omega_1, \quad (7)$$

$$-\nabla \cdot (\beta_2 \nabla \mathbf{u}_2) + \nabla p_2 = \mathbf{f}_2, \quad \text{in } \Omega_2, \quad (8)$$

$$\nabla \cdot \mathbf{u}_2 = 0, \quad \text{in } \Omega_2, \quad (9)$$

$$\mathbf{u}_1 = \mathbf{u}_2, \quad \text{on } \Gamma, \quad (10)$$

$$(\beta_1 \nabla \mathbf{u}_1 - p_1 \mathbf{I}) \mathbf{n}_1 + (\beta_2 \nabla \mathbf{u}_2 - p_2 \mathbf{I}) \mathbf{n}_2 = \mathbf{w}, \quad \text{on } \Gamma, \quad (11)$$

$$\mathbf{u}_1 = 0, \mathbf{u}_2 = 0, \quad \text{on } \partial\Omega \setminus \Gamma, \quad (12)$$

which can be considered as the linearized model of an immiscible two-phase fluid flow problem, where the primary variable pair (\mathbf{u}, p) satisfies $\mathbf{u}|_{\Omega_1} = \mathbf{u}_1$, $\mathbf{u}|_{\Omega_2} = \mathbf{u}_2$, $p|_{\Omega_1} = p_1$, $p|_{\Omega_2} = p_2$, which are associated with $\mathbf{f} \in (L^2(\Omega))^d$ satisfying $\mathbf{f}|_{\Omega_1} = \mathbf{f}_1 \in (L^2(\Omega_1))^d$, $\mathbf{f}|_{\Omega_2} = \mathbf{f}_2 \in (L^2(\Omega_2))^d$. The jump coefficient $\beta \in L^\infty(\Omega)$ satisfies $\beta|_{\Omega_1} = \beta_1 \in W^{1,\infty}(\Omega_1)$, $\beta|_{\Omega_2} = \beta_2 \in W^{1,\infty}(\Omega_2)$, $\beta_1 \neq \beta_2$.

And, the third type is the Stokes/elliptic interface problem, defined as

$$-\nabla \cdot (\beta_1 \nabla \mathbf{u}_1) + \nabla p_1 = \mathbf{f}_1, \quad \text{in } \Omega_1, \quad (13)$$

$$\nabla \cdot \mathbf{u}_1 = 0, \quad \text{in } \Omega_1, \quad (14)$$

$$-\nabla \cdot (\beta_2 \nabla \mathbf{u}_2) = \mathbf{f}_2, \quad \text{in } \Omega_2, \quad (15)$$

$$\mathbf{u}_1 = \mathbf{u}_2, \quad \text{on } \Gamma, \quad (16)$$

$$(\beta_1 \nabla \mathbf{u}_1 - p_1 \mathbf{I}) \mathbf{n}_1 + \beta_2 \nabla \mathbf{u}_2 \mathbf{n}_2 = \mathbf{w}, \quad \text{on } \Gamma, \quad (17)$$

$$\mathbf{u}_1 = 0, \mathbf{u}_2 = 0, \quad \text{on } \partial\Omega \setminus \Gamma, \quad (18)$$

which can be considered as a steady state linearized model of FSI problems, where, the primary variable pair (\mathbf{u}, p_1) satisfies $\mathbf{u}|_{\Omega_1} = \mathbf{u}_1$, $\mathbf{u}|_{\Omega_2} = \mathbf{u}_2$, $p_1 \in \Omega_1$, which are associated with $\mathbf{f} \in (L^2(\Omega))^d$ satisfying $\mathbf{f}|_{\Omega_1} = \mathbf{f}_1 \in (L^2(\Omega_1))^d$, $\mathbf{f}|_{\Omega_2} = \mathbf{f}_2 \in (L^2(\Omega_2))^d$. The jump coefficient $\beta \in L^\infty(\Omega)$ satisfies $\beta|_{\Omega_1} = \beta_1 \in W^{1,\infty}(\Omega_1)$, $\beta|_{\Omega_2} = \beta_2 \in W^{1,\infty}(\Omega_2)$, $\beta_1 \neq \beta_2$.

2.2 DLM/FD method for the elliptic interface problem

The main idea of the DLM/FD method is to smoothly extend one material, such as the fluid in FSI, into another material's subdomain, such as the structure in FSI, as a fictitious equation whose primary variable is constrained to equal to that of the occupied material's equation in its subdomain and on the interface too. And, such constraint is weakly imposed through the Lagrange multiplier (a pseudo body force) in the DLM/FD method. Thus, a monolithic saddle-point system is formed in regard to the Lagrange multiplier and primary variables, for which the classical Babuška–Brezzi's theory [4, 3] can be employed to prove the well-posedness, stability as well as convergence properties [2, 16]. In the following, we introduce the DLM/FD finite element method for each type of interface problem that is defined in Section 2.1.

Define $\mathbf{V}^E = H_0^1(\Omega)$, $\mathbf{V}_2^E = H^1(\Omega_2)$, $\mathbf{A}^E = (\mathbf{V}_2^E)^*$, where $(\mathbf{V}_2^E)^*$ denotes the dual space of \mathbf{V}_2^E . Let $T_h(\Omega)$ and $T_H(\Omega_2)$ be the meshes of Ω and Ω_2 , respectively. And denote by \mathbf{V}_h^E , $\mathbf{V}_{2,H}^E$ and \mathbf{A}_H^E the conforming finite element spaces of \mathbf{V}^E , \mathbf{V}_2^E and \mathbf{A}^E , respectively. Here and hereafter, let $(\cdot, \cdot)_\omega$ be the L^2 inner product over ω , and $\langle \cdot, \cdot \rangle_\omega$ be the dual product over ω that is actually associated with the H^1 inner product [1].

Then, the DLM/FD finite element method for solving elliptic interface problem (1)-(5) can be defined as follows [2, 1]: Find $(\tilde{u}_h, u_{2,H}, \lambda_H) \in \mathbf{V}_h^E \times \mathbf{V}_{2,H}^E \times \mathbf{A}_H^E$ such that

$$(\tilde{\beta} \nabla \tilde{u}_h, \nabla v_h)_\Omega + \langle \lambda_H, v_h|_{\Omega_2} \rangle_{\Omega_2} = (\tilde{f}, v_h)_\Omega, \quad (19)$$

$$\left((\beta_2 - \tilde{\beta}) \nabla u_{2,H}, \nabla v_{2,H} \right)_{\Omega_2} - \langle \lambda_H, v_{2,H} \rangle_{\Omega_2} = \left(f_2 - \tilde{f}_2, v_{2,H} \right)_{\Omega_2} + (w, v_{2,H})_\Gamma, \quad (20)$$

$$\langle \xi_H, \tilde{u}_h|_{\Omega_2} - u_{2,H} \rangle_{\Omega_2} = 0, \forall (v_h, v_{2,H}, \xi) \in \mathbf{V}_h^E \times \mathbf{V}_{2,H}^E \times \mathbf{A}_H^E. \quad (21)$$

2.3 DLM/FD method for the Stokes interface problem

Define $\mathbf{V}^S = (H_0^1(\Omega))^d$, $\mathbf{Q}^S = L^2(\Omega)$, $\mathbf{V}_2^S = (H^1(\Omega_2))^d$, $\mathbf{A}^S = (\mathbf{V}_2^S)^*$, where $(\mathbf{V}_2^S)^*$ denotes the dual space of \mathbf{V}_2^S . Let \mathbf{V}_h^S , $\mathbf{V}_{2,H}^S$, \mathbf{Q}_h^S and \mathbf{A}_H^S be the conforming finite element spaces of \mathbf{V}^S , \mathbf{V}_2^S , \mathbf{Q}^S and \mathbf{A}^S , respectively. Then, the DLM/FD finite element method for solving the Stokes interface problem (6)-(12) can be defined as follows [13]: Find $(\tilde{\mathbf{u}}_h, \mathbf{u}_{2,H}, \tilde{p}_h, \boldsymbol{\lambda}_H) \in \mathbf{V}_h^S \times \mathbf{V}_{2,H}^S \times \mathbf{Q}_h^S \times \mathbf{A}_H^S$ such that

$$(\tilde{\beta} \nabla \tilde{\mathbf{u}}_h, \nabla \mathbf{v}_h)_\Omega - (\tilde{p}_h, \nabla \cdot \mathbf{v}_h)_\Omega + \langle \boldsymbol{\lambda}_H, \mathbf{v}_h|_{\Omega_2} \rangle_{\Omega_2} = (\tilde{\mathbf{f}}, \mathbf{v}_h)_\Omega, \quad (22)$$

$$(\nabla \cdot \tilde{\mathbf{u}}_h, q_h)_\Omega = 0, \quad (23)$$

$$\left((\beta_2 - \tilde{\beta}) \nabla \mathbf{u}_{2,H}, \nabla \mathbf{v}_{2,H} \right)_{\Omega_2} - \langle \boldsymbol{\lambda}_H, \mathbf{v}_{2,H} \rangle_{\Omega_2} = \left(\mathbf{f}_2 - \tilde{\mathbf{f}}_2, \mathbf{v}_{2,H} \right)_{\Omega_2} + (\mathbf{w}, \mathbf{v}_{2,H})_\Gamma, \quad (24)$$

$$\langle \boldsymbol{\xi}_H, \tilde{\mathbf{u}}_h|_{\Omega_2} - \mathbf{u}_{2,H} \rangle_{\Omega_2} = 0, \forall (\mathbf{v}_h, \mathbf{v}_{2,H}, q_h, \boldsymbol{\xi}_H) \in \mathbf{V}_h^S \times \mathbf{V}_{2,H}^S \times \mathbf{Q}_h^S \times \mathbf{A}_H^S. \quad (25)$$

2.4 DLM/FD method for the Stokes/elliptic interface problem

The spaces to be used for defining the weak formulation and the DLM/FD formulation of Stokes/elliptic interface problem are the same as those of Stokes interface problem. The DLM/FD finite element method is proposed and analyzed in [15] for the Stokes/elliptic interface problem (13)-(18), as described below.

Find $(\tilde{\mathbf{u}}_h, \mathbf{u}_{2,H}, \tilde{p}_h, \boldsymbol{\lambda}_H) \in \mathbf{V}_h^S \times \mathbf{V}_{2,H}^S \times \mathbf{Q}_h^S \times \mathbf{A}_H^S$ such that

$$(\tilde{\beta} \nabla \tilde{\mathbf{u}}_h, \nabla \mathbf{v}_h)_\Omega - (\tilde{p}_h, \nabla \cdot \mathbf{v}_h)_\Omega + \langle \boldsymbol{\lambda}_H, \mathbf{v}_h|_{\Omega_2} \rangle_{\Omega_2} = (\tilde{\mathbf{f}}, \mathbf{v}_h)_\Omega, \quad (26)$$

$$(\nabla \cdot \tilde{\mathbf{u}}_h, q_h)_\Omega - (\nabla \cdot \mathbf{u}_{2,H}, q_h)_{\Omega_2} = 0, \quad (27)$$

$$\begin{aligned} & \left((\beta_2 - \tilde{\beta}) \nabla \mathbf{u}_{2,H}, \nabla \mathbf{v}_{2,H} \right)_{\Omega_2} + (p_h|_{\Omega_2}, \nabla \cdot \mathbf{v}_{2,H})_{\Omega_2} \\ & - \langle \boldsymbol{\lambda}_H, \mathbf{v}_{2,H} \rangle_{\Omega_2} = \left(\mathbf{f}_2 - \tilde{\mathbf{f}}|_{\Omega_2}, \mathbf{v}_{2,H} \right)_{\Omega_2} + (\mathbf{w}, \mathbf{v}_{2,H})_\Gamma, \end{aligned} \quad (28)$$

$$\langle \boldsymbol{\xi}_H, \tilde{\mathbf{u}}_h|_{\Omega_2} - \mathbf{u}_{2,H} \rangle_{\Omega_2} = 0, \forall (\mathbf{v}_h, \mathbf{v}_{2,H}, q_h, \boldsymbol{\xi}_H) \in \mathbf{V}_h^S \times \mathbf{V}_{2,H}^S \times \mathbf{Q}_h^S \times \mathbf{A}_H^S. \quad (29)$$

3 Numerical integration schemes

Note that in the DLM/FD finite element methods described in Sections 2.2-2.4, some inner product terms involve an integration over the immersed domain Ω_2 with a product of two piecewise functions defined on $T_h(\Omega)$ and $T_H(\Omega_2)$, respectively. For instance,

$$\langle \boldsymbol{\lambda}_H, \mathbf{v}_h|_{\Omega_2} \rangle_{\Omega_2} \text{ in (19) and } \langle \boldsymbol{\xi}_H, \tilde{\mathbf{u}}_h|_{\Omega_2} \rangle_{\Omega_2} \text{ in (21),} \quad (30)$$

$$\langle \boldsymbol{\lambda}_H, \mathbf{v}_h|_{\Omega_2} \rangle_{\Omega_2} \text{ in (22) and } \langle \boldsymbol{\xi}_H, \tilde{\mathbf{u}}_h|_{\Omega_2} \rangle_{\Omega_2} \text{ in (25),} \quad (31)$$

$$(\nabla \cdot \tilde{\mathbf{u}}_{2,H}, q_h)_{\Omega_2} \text{ in (26) and } (p_h|_{\Omega_2}, \nabla \cdot \mathbf{v}_{2,H})_{\Omega_2} \text{ in (29).} \quad (32)$$

Since two grids $T_h(\Omega)$ and $T_H(\Omega_2)$ are constructed independently, they are generally not matched with each other, see Figure 2. Thus, we need to employ some numerical techniques to implement the numerical integration for terms shown in (30)-(32) in order to make the DLM/FD finite element method perform well. In this paper, we restrict ourselves to the cases of triangular finite element.

It shall be pointed out that we can not simply make such a conclusion that the higher order the integration scheme, the higher accuracy the numerical integration. That is because the integrand functions shown in (30)-(32) are essentially the product of piecewise polynomials defined on two non-matched meshes, $T_h(\Omega)$ or $T_H(\Omega_2)$, inducing an insufficiently smooth integrand function in each element of $T_H(\Omega_2)$, and thus it is not able to deduce a higher order derivative in the remainder of the numerical integration scheme.

3.1 Commonly-used numerical integration schemes

The numerical integration schemes in the field of finite element method are of the form: $\int_{\hat{K}} f(\hat{x})d\hat{x} = \sum_i \omega_i f(\lambda_i)$, where \hat{K} stands for the reference element that is an isosceles right triangle with two sides equal 1, that is, three vertices of \hat{K} are $(0, 0)$, $(1, 0)$ and $(0, 1)$. And, the quadrature points are denoted by the barycentric coordinates. Ten different commonly-used numerical integration schemes, from Scheme 1 to Scheme 9 as listed in the Appendix, are adopted to carry out our numerical studies in Section 4.

Moreover, to improve the numerical integration accuracy, we consider the compound type formulas of numerical integration, for which each triangular reference element is divided into four equilateral sub-triangles. For example, Scheme 4c1 can be obtained by applying Scheme 4 of the numerical integration to each one of four sub-triangles in the first-time refinement of the reference element, Scheme 4c2 is constructed by applying Scheme 4 to each one of 16 sub-triangles after refining the reference element twice, and Scheme 4c3 based on Scheme 4 and 64 sub-triangles after refining the reference element for three times, and so forth, which are not necessarily shown in the Appendix for the simplicity.

3.2 The subgrid integration scheme

The subgrid integration scheme has been proposed and used in [18] for solving two-dimensional parabolic interface problems with the DLM/FD method. The main ingredient of this scheme is to generate a subgrid, $T_H^r(\Omega_2)$, by finding all intersections of $T_h(\Omega)$ and $T_H(\Omega_2)$ then forming a new subgrid structure in the immersed domain Ω_2 . Clearly, $T_H^r(\Omega_2)$ is a matching subset of both $T_h(\Omega)$ and $T_H(\Omega_2)$, and $T_H^r(\Omega_2)$ is a finer mesh on Ω_2 . Thus, all integral terms as shown in (30)-(32) can be implemented on $T_H^r(\Omega_2)$ now, and the piecewise polynomial defined on $T_H^r(\Omega_2) \subset T_h(\Omega)$ must be also piecewisely smooth on $T_H(\Omega_2)$. Then, the interpolations between two different meshes are avoided. An example of such a subgrid is shown in Figure 2.

Since the integrand function on each element of the subgrid $T_H^r(\Omega_2)$ is smooth, the commonly-used integration schemes with the help of such a subgrid can yield sufficiently high accuracy for numerical integrations. In this sense, the subgrid integration scheme is of the highest accuracy among the schemes presented in this paper, as long as a subtle implementation programming can be done to eliminate every possible geometrical error when finding the intersection points of two non-matching meshes. Interested readers can refer to [18] for more details about the subgrid integration scheme and its implementation.

4 Numerical Experiments

In what follows, we will carry out two scenarios in our numerical experiments to investigate effects of different numerical integration schemes on the approximation solutions of the DLM/FD finite element method for solving three types of steady interface problems: (1) the real solution of the original interface problem is unknown; (2) the real solution of the original interface problem is known.

To that end, a fixed mesh size is chosen as $h = 1/64$ and $H = 1/64$ to attain two meshes $T_h(\Omega)$ and $T_H(\Omega_2)$, as depicted in Figure 2. On these two fixed meshes,

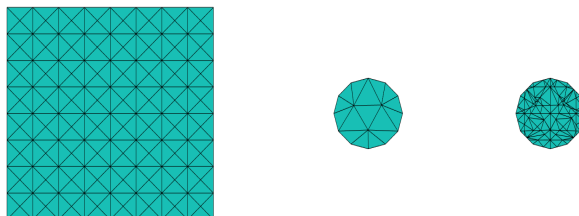


Fig. 2. The meshes (from left to right): the background mesh $T_h(\Omega)$ partitioned in a square Ω , the foreground mesh $T_H(\Omega_2)$ partitioned in a disk Ω_2 , and the subgrid $T_H^r(\Omega_2)$ in Ω_2 .

we will implement the DLM/FD finite element method with different numerical integration schemes for the elliptic-, Stokes-, and Stokes/elliptic-interface problems, respectively.

4.1 The scenario of unknown real solutions

In this scenario, since the real solution is unknown, we will report the energy norm of the numerical solution instead of its approximation error to the real solution, and compare all numerical solutions in the energy norm obtained from different numerical integration schemes for each type of interface problem.

The elliptic interface problem with a unknown real solution Let Ω be a square with the size $(0, 6) \times (0, 6)$ and Ω_2 be a unit circle with the center at $(3, 3)$. Consider the elliptic interface problem (1)-(5) with the following jump coefficients and right hand side functions:

- Case E1: $\beta_1 = 1$, $\beta_2 = 100$, $f_1 = f_2 = 1$,
- Case E2: $\beta_1 = 1$, $\beta_2 = 10000$, $f_1 = f_2 = 1$.

The linear (P_1) finite element space is adopted to define \mathbf{V}_h^E , $\mathbf{V}_{2,H}^E$ and Λ_H^E , which are used in the implementation of the DLM/FD finite element method (19)-(21). Numerical solutions in H^1 -norm in regard to different numerical integration schemes are reported in Tables 1-2 for two cases E1-E2, where, we use the numbers from 1 to 9 to successively represent nine commonly-used non-compound type numerical integration schemes, use the notation “4c1”, “4c2” and “4c3” to represent three compound-type formula of numerical integration, respectively, and use “s” to stand for the subgrid integration scheme.

Table 1. Numerical results of Case E1

schemes #	1	2	3	4	5	6	7
$\ \tilde{u}_h\ _1$	1.1057e+1	1.1057e+1	1.1057e+1	1.1057e+1	1.1057e+1	1.1057e+1	1.1057e+1
scheme #	8	9	4c1	4c2	4c3	s	
$\ \tilde{u}_h\ _1$	1.1057e+1	1.1057e+1	1.1057e+1	1.1057e+1	1.1058e+1	1.1057e+1	

Table 2. Numerical results of Case E2

schemes #	1	2	3	4	5	6	7
$\ \tilde{u}_h\ _1$	1.1055e+1	1.1052e+1	1.1054e+1	1.1051e+1	1.1052e+1	1.1052e+1	1.1052e+1
scheme #	8	9	4c1	4c2	4c3	s	
$\ \tilde{u}_h\ _1$	1.1052e+1	1.1052e+1	1.1052e+1	1.1053e+1	1.1052e+1	1.1051e+1	

From Tables 1-2, we find out all numerical integration schemes yield almost the same numerical solution in terms of the energy (H^1 -) norm, that is even true for the case of large jump coefficients. Thus, the DLM/FD finite element

method for the elliptic interface problem is insensitive with different numerical integration schemes, i.e., all commonly-used numerical integration schemes and their compound formulas can achieve the same approximation accuracy with the subgrid integration scheme which supposes to produce the highest accuracy of the numerical integration for the DLM/FD method.

The Stokes interface problem with a unknown real solution Let Ω be a square with the size $(0, 1) \times (0, 1)$ and Ω_2 be a circle with the center at $(0.3, 0.3)$ and the radius 0.1. Consider the Stokes interface problem (6)-(12) with the following jump coefficients and right hand side functions:

- Case S1: $\beta_1 = 1, \beta_2 = 100, \mathbf{f}_1 = (e^x, e^y)^T, \mathbf{f}_2 = (0, 0)^T$.
- Case S2: $\beta_1 = 1, \beta_2 = 10000, \mathbf{f}_1 = (e^x, e^y)^T, \mathbf{f}_2 = (0, 0)^T$.

Table 3. Numerical results of Case S1

schemes #	2	3	4	5	6	7
$\ \tilde{\mathbf{u}}_h\ _1$	1.7091e-2	1.8972e-2	1.8557e-2	1.8417e-2	1.8500e-2	1.8570e-2
$\ p_h\ _0$	2.0895e+0	2.0883e+0	2.0884e+0	2.0884e+0	2.0884e+0	2.0884e+0
schemes #	8	9	4c1	4c2	4c3	s
$\ \tilde{\mathbf{u}}_h\ _1$	1.8328e-2	1.8221e-2	1.8197e-2	1.7985e-2	1.7917e-2	1.7047e-2
$\ p_h\ _0$	2.0885e+0	2.0886e+0	2.0885e+0	2.0886e+0	2.0886e+0	2.0892e+0

Table 4. Numerical results of Case S2

schemes #	2	3	4	5	6	7
$\ \tilde{\mathbf{u}}_h\ _1$	1.6789e-2	1.8964e-2	1.8537e-2	1.8396e-2	1.8475e-2	1.8544e-2
$\ p_h\ _0$	2.0903e+0	2.0883e+0	2.0884e+0	2.0884e+0	2.0884e+0	2.0884e+0
schemes #	8	9	4c1	4c2	4c3	s
$\ \tilde{\mathbf{u}}_h\ _1$	1.8302e-2	1.8188e-2	1.8164e-2	1.7944e-2	1.7873e-2	1.7043e-2
$\ p_h\ _0$	2.0886e+0	2.0886e+0	2.0885e+0	2.0887e+0	2.0887e+0	2.0897e+0

The Taylor-Hood P_2P_1 -mixed finite element is adopted to define $\mathbf{V}_h^S, \mathbf{V}_{2,H}^S, \mathbf{Q}_h^S$ and \mathbf{A}_H^S , which are used in the implementation of the DLM/FD finite element method (22)-(25). Numerical solutions in the energy norm (the velocity in H^1 -norm and the pressure in L^2 -norm) in regard to different numerical integration schemes are reported in Tables 3-4 for two cases S1-S2. From these tables, we observe some obvious differences on the numerical solutions of velocity between different numerical integration schemes, while the numerical pressure is insensitive with different integration schemes.

The Stokes/elliptic interface problem with a unknown real solution

Let Ω be a square with the size $(0, 1) \times (0, 1)$ and Ω_2 be a circle with the center at $(0.3, 0.3)$ and the radius 0.1. Consider the Stokes/elliptic interface problem (13)-(18) with the following jump coefficients and right hand side functions:

- Case SE1: $\beta_1 = 1, \beta_2 = 100, \mathbf{f}_1 = \mathbf{f}_2 = (1, 1)^T$,
- Case SE2: $\beta_1 = 1, \beta_2 = 10000, \mathbf{f}_1 = \mathbf{f}_2 = (1, 1)^T$.

The same P_2P_1 -mixed finite element space is adopted to define $\mathbf{V}_h^S, \mathbf{V}_{2,H}^S, \mathbf{Q}_h^S$ and \mathbf{A}_H^S , which are used in the implementation of the DLM/FD finite element method (26)-(29). Numerical solutions in the energy norm in regard to different numerical integration schemes are reported in Tables 5-6 for two cases SE1-SE2, from which the similar conclusions can be drawn as those for the numerical results of Stokes interface problem in Cases S1-S2.

Table 5. Numerical results of Case SE1

schemes #	2	3	4	5	6	7
$\ \tilde{\mathbf{u}}_h\ _1$	1.8780e-2	1.8979e-2	1.8559e-2	1.8420e-2	1.8497e-2	1.8567e-2
schemes #	8	9	4c1	4c2	4c3	s
$\ \tilde{\mathbf{u}}_h\ _1$	1.8325e-2	1.8215e-2	1.8191e-2	1.7973e-2	1.7902e-2	1.7105e-2

Table 6. Numerical results of Case SE2

schemes #	2	3	4	5	6	7
$\ \tilde{\mathbf{u}}_h\ _1$	1.8763e-2	1.8964e-2	1.8537e-2	1.8396e-2	1.8475e-2	1.8544e-2
schemes #	8	9	4c1	4c2	4c3	s
$\ \tilde{\mathbf{u}}_h\ _1$	1.8302e-02	1.8188e-2	1.8164e-2	1.7944e-2	1.7873e-2	1.7098e-2

4.2 The scenario of known and smooth real solutions

The elliptic interface problem with a known real solution Let Ω be a square with the size $(0, 6) \times (0, 6)$ and Ω_2 be a unit circle with the center at $(3, 3)$. Consider the elliptic interface problem (1)-(5) with the following jump coefficients and right hand side functions:

- Case E3: $\beta_1 = 1$, $\beta_2 = 100$, f_1 and f_2 are defined below;
- Case E4: $\beta_1 = 1$, $\beta_2 = 10000$, f_1 and f_2 are defined below,

where, f_1 and f_2 are chosen such that the real solution of (1)-(5) is taken as $u = (x - 6)x(y - 6)y((x - 3)^2 + (y - 3)^2 - 1)^2$.

Table 7. Numerical results of Case E3

scheme #	1	2	3	4	5	6	7
$\ u - \tilde{u}_h\ _1$	2.0333e+2	2.0330e+2	2.0330e+2	2.0329e+2	2.0329e+2	2.0329e+2	2.0329e+2
scheme #	8	9	4c1	4c2	4c3	s	
$\ u - \tilde{u}_h\ _1$	2.0329e+2	2.0329e+2	2.0329e+2	2.0329e+2	2.0338e+2	2.0329e+2	

Table 8. Numerical results of Case E4

scheme #	1	2	3	4	5	6	7
$\ u - \tilde{u}_h\ _1$	5.3984e+2	5.3830e+2	5.396e+2	5.3805e+2	5.3801e+2	5.3803e+2	5.3804e+2
scheme #	8	9	4c1	4c2	4c3	s	
$\ u - \tilde{u}_h\ _1$	5.3802e+2	5.3802e+2	5.3800e+2	5.3800e+2	5.3801e+2	5.3801e+2	

With the P_1 finite element space, the numerical results of the DLM/FD finite element method (19)-(21) are reported in Tables 7-8 for two cases E3-E4, from which we observe that all numerical errors in H^1 -norm in regard to different numerical integration schemes are almost the same, confirming again that the DLM/FD finite element method for the elliptic interface problem is insensitive with different numerical integration schemes.

The Stokes interface problem with a known real solution Let Ω be a square with the size $(0, 1) \times (0, 1)$ and Ω_2 be a circle with the center at $(0.3, 0.3)$ and the radius 0.1. Consider the Stokes interface problem (6)-(12) with the following jump coefficients and right hand side functions:

- Case S3: $\beta_1 = 1$, $\beta_2 = 100$, \mathbf{f}_1 and \mathbf{f}_2 are defined below;
- Case S4: $\beta_1 = 1$, $\beta_2 = 10000$, \mathbf{f}_1 and \mathbf{f}_2 are defined below,

where, \mathbf{f}_1 and \mathbf{f}_2 are chosen such that the real solution of (6)-(12) can be taken as

$$\mathbf{u} = \begin{pmatrix} \frac{(y-0.3)((x-0.3)^2+(y-0.3)^2-0.01)}{\beta_{i_2}} \\ -\frac{(x-0.3)((x-0.3)^2+(y-0.3)^2-0.01)}{\beta_i} \end{pmatrix} \quad \text{if } (x, y)^T \in \Omega_i,$$

$$p = 0.01(x^3 - y^3).$$

Note that an inhomogeneous boundary condition is employed instead for the Stokes interface problem in the above two cases.

With the P_2P_1 -mixed finite element space, the numerical results of the DLM/FD finite element method (22)-(25) are reported in Tables 9-10 for two

cases S3-S4, from which we observe the obvious differences on numerical solutions of both the velocity and the pressure between different numerical integration schemes, and, the subgrid integration scheme produces the lowest approximation error, i.e., the best accuracy, for both the velocity and the pressure in comparison with other numerical integration schemes in all two cases.

To look into effects of other numerical integration schemes than the subgrid scheme, in terms of the following formula

$$\frac{\|\mathbf{u} - \tilde{\mathbf{u}}_h^i\|_1 - \|\mathbf{u} - \tilde{\mathbf{u}}_h^s\|_1}{\|\mathbf{u} - \tilde{\mathbf{u}}_h^s\|_1} \text{ or } \frac{\|\mathbf{u} - \tilde{\mathbf{u}}_h^{5ci}\|_1 - \|\mathbf{u} - \tilde{\mathbf{u}}_h^s\|_1}{\|\mathbf{u} - \tilde{\mathbf{u}}_h^s\|_1},$$

$$\frac{\|p - p_h^i\|_0 - \|p - p_h^s\|_0}{\|p - p_h^s\|_0} \text{ or } \frac{\|p - p_h^{5ci}\|_0 - \|p - p_h^s\|_0}{\|p - p_h^s\|_0},$$

we calculate and plot the relative differences between numerical errors obtained from other integration schemes and those from the subgrid scheme, as shown in Figure 3, where, two cases illustrate a slow convergence tendency on numerical errors of the velocity towards those from the subgrid scheme along with the increase of numerical integration scheme number. However, such tendency does not even apply to numerical errors of the pressure, instead, Figure 3 shows that a higher order integration scheme may lead to a worse approximation to the pressure. Furthermore, in Figure 4, a special case is observed that the numerical solution obtained by Scheme 2 is significantly polluted inside Ω_2 while the numerical solution obtained by the subgrid integration scheme is of better accuracy in Ω_2 , which implies that the Lagrange multiplier does not work well to enforce (25) hold true, reflecting from the low accuracy of Scheme 2.

Table 9. Numerical results of Case S3

scheme #	2	3	4	5	6	7
$\ \mathbf{u} - \tilde{\mathbf{u}}_h\ _1$	1.8194e-3	1.5948e-3	1.6239e-3	1.5642e-3	1.6210e-3	1.6269e-3
$\ p - p_h\ _0$	5.9637e-1	6.1253e-1	7.2035e-1	7.0451e-1	8.3067e-1	7.9560e-1
scheme #	8	9	4c1	4c2	4c3	s
$\ \mathbf{u} - \tilde{\mathbf{u}}_h\ _1$	1.6024e-3	1.5858e-3	1.6295e-3	1.5737e-3	1.5595e-3	7.8025e-4
$\ p - p_h\ _0$	7.7359e-1	7.9780e-1	8.5104e-1	8.8010e-1	8.8306e-1	4.4222e-1

Table 10. Numerical results of Case S4

scheme #	2	3	4	5	6	7
$\ \mathbf{u} - \tilde{\mathbf{u}}_h\ _1$	1.8718e-3	1.7913e-3	1.9442e-3	1.9896e-3	2.0783e-3	2.0616e-3
$\ p - p_h\ _0$	4.8900e-1	5.6678e-1	5.4602e-1	5.5996e-1	6.2313e-1	6.2266e-1
scheme #	8	9	5c1	5c2	5c3	s
$\ \mathbf{u} - \tilde{\mathbf{u}}_h\ _1$	2.0758e-3	2.0257e-3	2.0505e-3	2.0818e-3	2.0549e-3	1.2073e-3
$\ p - p_h\ _0$	5.7456e-1	5.7665e-1	6.2303e-1	6.2144e-1	6.2582e-1	4.3039e-1

The Stokes/elliptic interface problem with a known real solution Let Ω be a square with the size $(0, 1) \times (0, 1)$ and Ω_2 be a circle with the center at $(0.3, 0.3)$ and the radius 0.1. Consider the Stokes/elliptic interface problem (13)-(18) with the following jump coefficients and right hand side functions:

- Case SE3: $\beta_1 = 1$, $\beta_2 = 100$, \mathbf{f}_1 and \mathbf{f}_2 are defined below;
- Case SE4: $\beta_1 = 1$, $\beta_2 = 10000$, \mathbf{f}_1 and \mathbf{f}_2 are defined below,

where, \mathbf{f}_1 and \mathbf{f}_2 are chosen such that the real solution of (13)-(18) is taken as

$$\mathbf{u} = \begin{pmatrix} \frac{(y-0.3)((x-0.3)^2+(y-0.3)^2-0.01)}{\beta_{i_2}} \\ \frac{-(x-0.3)((x-0.3)^2+(y-0.3)^2-0.01)}{\beta_i} \end{pmatrix} \quad \text{if } (x, y)^T \in \Omega_i,$$

$$p = 0.01(x^3 - y^3)((x - 0.3)^2 + (y - 0.3)^2 - 0.01).$$

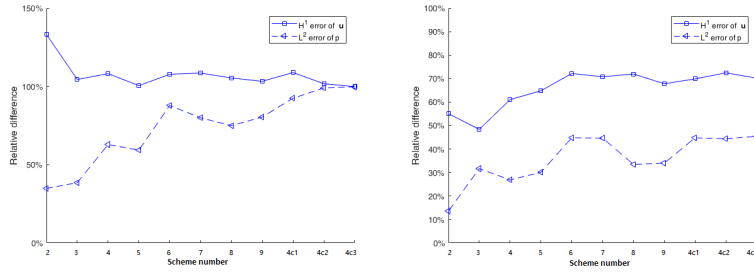


Fig. 3. Relative differences of the velocity error in H^1 -norm and of the pressure error in L^2 -norm for Cases S3 and S4 (from left to right).

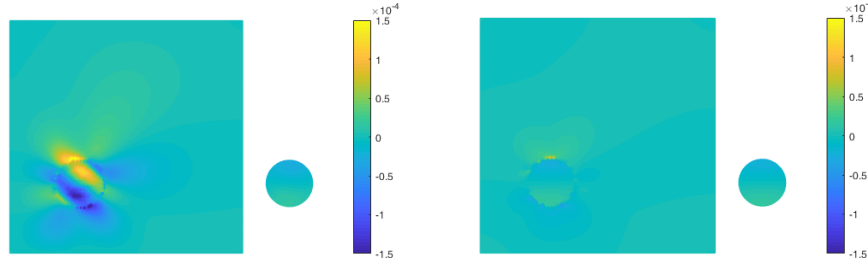


Fig. 4. The first components of $\mathbf{u} - \tilde{\mathbf{u}}_h^2$ and $\mathbf{u}_2 - \mathbf{u}_{2,H}^2$ vs the first components of $\mathbf{u} - \tilde{\mathbf{u}}_h^s$ and $\mathbf{u}_2 - \mathbf{u}_{2,H}^s$ for Cases S3 (from left to right).

Note that an inhomogeneous boundary condition is employed instead for the Stokes/elliptic interface problem in the above two cases.

With the P_2P_1 -mixed finite element space, the numerical results of the DLM/FD finite element method (26)-(29) are reported in Tables 11-12 and Figure 5 for two cases SE3-SE4, from which the same conclusions can be drawn as those for the numerical velocity errors of Stokes interface problem in Cases S3-S4, and, the slowly convergent relative differences of $\|\tilde{\mathbf{u}} - \tilde{\mathbf{u}}_h\|_1$, that is generally between 20% and 60%, can be observed in Figure 5.

Table 11. Numerical results of Case SE3

scheme #	2	3	4	5	6	7
$\ \mathbf{u} - \tilde{\mathbf{u}}_h\ _1$	1.6099e-3	1.5944e-3	1.6228e-3	1.5636e-3	1.6225e-3	1.6268e-3
scheme #	8	9	5c1	5c2	5c3	s
$\ \mathbf{u} - \tilde{\mathbf{u}}_h\ _1$	1.6049e-3	1.5898e-3	1.6364e-3	1.5855e-3	1.5729e-3	1.0022e-3

Table 12. Numerical results of Case SE4

scheme #	2	3	4	5	6	7
$\ \mathbf{u} - \tilde{\mathbf{u}}_h\ _1$	1.8389e-3	1.7904e-3	1.9435e-3	1.9891e-3	2.0779e-3	2.0612e-3
scheme #	8	9	5c1	5c2	5c3	s
$\ \mathbf{u} - \tilde{\mathbf{u}}_h\ _1$	2.0755e-3	2.0251e-3	2.0502e-3	2.0813e-3	2.0543e-3	1.5111e-3

In summary, we notice that for the elliptic-, Stokes- and Stokes/elliptic- interface problem, their coefficient matrices of the linear algebra systems obtained by the DLM/FD FEM are in the following forms, respectively

$$S_E = \begin{pmatrix} A & O & B^T \\ O & A_2 & C^T \\ B & C & O \end{pmatrix}, \quad S_S = \begin{pmatrix} A & O & B^T & C^T \\ O & A_2 & O & D^T \\ B & O & O & O \\ C & D & O & O \end{pmatrix}, \quad S_{SE} = \begin{pmatrix} A & O & B^T & C^T \\ O & A_2 & E & D^T \\ B & -E & O & O \\ C & D & O & O \end{pmatrix}, \quad (33)$$

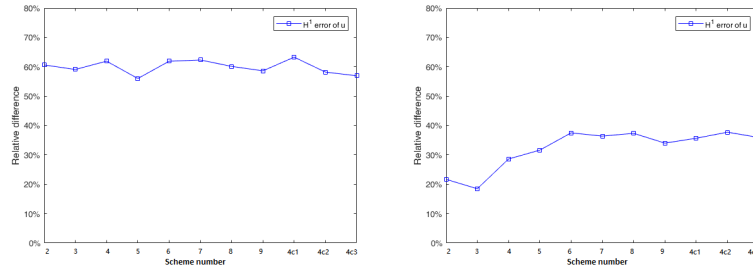


Fig. 5. Relative differences of the velocity error in H^1 -norm for Cases SE3 and SE4 (from left to right).

where “ O ” denotes the zero matrix block. One way to view these linear algebra systems as saddle point problems is to split the matrices as showed in (33), where the Lagrange multiplier and the pressure are bundled in S_S and S_{SE} . Slight changes of B in S_E , C in S_S , C and E in S_{SE} may result in quite different effects on the corresponding numerical solutions, which is a possible reason for explaining the observations illustrated in the previous sections: the DLM/FD FEM is insensitive with various numerical integration schemes for the elliptic interface problem, however, it is sensitive with different numerical integration schemes for both the Stokes- and the Stokes/elliptic interface problems. Although only two-dimensional interface problems are considered in the numerical experiments, the DLM/FD FEM and subgrid integration technique can be used for solving the interface problems in any dimension.

5 Conclusions

In this paper, we study the effects of different numerical integration schemes, including the commonly-used integration schemes and their compound-type schemes, and the subgrid integration scheme, on the performance of the DLM/FD finite element method for solving the elliptic-, Stokes-, and Stokes/elliptic-interface problem. Numerical experiments illustrate that: (1) DLM/FD FEM is insensitive with various numerical integration schemes for the elliptic interface problem; (2) DLM/FD FEM is sensitive with different numerical integration schemes for both Stokes- and Stokes/elliptic interface problem, and sometimes, numerical solutions obtained from other integration schemes than the subgrid integration scheme may not be reliable; (3) the subgrid integration scheme always results in numerical solutions with the best accuracy.

Appendix: Numerical Integration Schemes

Scheme #	λ_i	ω_i
1	(0.3333333333333333, 0.3333333333333333, 0.3333333333333333)	1.0000000000000000
2	(0.6666666666666667, 0.1666666666666667, 0.1666666666666667)	0.3333333333333333
	(0.1666666666666667, 0.6666666666666667, 0.1666666666666667)	0.3333333333333333
	(0.1666666666666667, 0.1666666666666667, 0.6666666666666667)	0.3333333333333333
3	(0.3333333333333333, 0.3333333333333333, 0.3333333333333333)	-0.5625000000000000
	(0.6000000000000000, 0.2000000000000000, 0.2000000000000000)	0.5208333333333333
	(0.2000000000000000, 0.6000000000000000, 0.2000000000000000)	0.5208333333333333
	(0.2000000000000000, 0.2000000000000000, 0.6000000000000000)	0.5208333333333333

Scheme #	λ_i	ω_i
4	(0.108103018168070, 0.445948490915965, 0.445948490915965) (0.445948490915965, 0.108103018168070, 0.445948490915965) (0.445948490915965, 0.445948490915965, 0.108103018168070) (0.816847572980459, 0.091576213509771, 0.091576213509771) (0.091576213509771, 0.816847572980459, 0.091576213509771) (0.091576213509771, 0.091576213509771, 0.816847572980459)	0.223381589678011 0.223381589678011 0.223381589678011 0.109951743655322 0.109951743655322 0.109951743655322
5	(0.333333333333333, 0.333333333333333, 0.333333333333333) (0.059715871789770, 0.470142064105115, 0.470142064105115) (0.470142064105115, 0.059715871789770, 0.470142064105115) (0.470142064105115, 0.470142064105115, 0.059715871789770) (0.797426985353087, 0.101286507323456, 0.101286507323456) (0.101286507323456, 0.797426985353087, 0.101286507323456) (0.101286507323456, 0.101286507323456, 0.797426985353087)	0.225000000000000 0.132394152788506 0.132394152788506 0.132394152788506 0.125939180544827 0.125939180544827 0.125939180544827
6	(0.249286745170910, 0.249286745170910, 0.501426509658179) (0.249286745170910, 0.501426509658179, 0.249286745170911) (0.501426509658179, 0.249286745170910, 0.249286745170911) (0.063089014491502, 0.063089014491502, 0.873821971016996) (0.063089014491502, 0.873821971016996, 0.063089014491502) (0.873821971016996, 0.063089014491502, 0.063089014491502) (0.310352451033784, 0.636502499121399, 0.053145049844817) (0.636502499121399, 0.053145049844817, 0.310352451033784) (0.053145049844817, 0.310352451033784, 0.636502499121399) (0.636502499121399, 0.310352451033784, 0.053145049844817) (0.310352451033784, 0.053145049844817, 0.636502499121399) (0.053145049844817, 0.636502499121399, 0.310352451033784)	0.116786275726379 0.116786275726379 0.116786275726379 0.050844906370207 0.050844906370207 0.050844906370207 0.082851075618374 0.082851075618374 0.082851075618374 0.082851075618374 0.082851075618374
7	(0.333333333333333, 0.333333333333333, 0.333333333333334) (0.260345966079040, 0.260345966079040, 0.479308067841920) (0.260345966079040, 0.479308067841920, 0.260345966079040) (0.479308067841920, 0.260345966079040, 0.260345966079040) (0.065130102902216, 0.065130102902216, 0.869739794195568) (0.065130102902216, 0.869739794195568, 0.065130102902216) (0.869739794195568, 0.065130102902216, 0.065130102902216) (0.312865496004874, 0.638444188569810, 0.048690315425316) (0.638444188569810, 0.048690315425316, 0.312865496004874) (0.048690315425316, 0.312865496004874, 0.638444188569810) (0.638444188569810, 0.312865496004874, 0.048690315425316) (0.312865496004874, 0.048690315425316, 0.638444188569810) (0.048690315425316, 0.638444188569810, 0.312865496004874)	-0.149570044467682 0.175615257433208 0.175615257433208 0.175615257433208 0.053347235608838 0.053347235608838 0.053347235608838 0.077113760890257 0.077113760890257 0.077113760890257 0.077113760890257 0.077113760890257
8	(0.333333333333333, 0.333333333333333, 0.333333333333334) (0.081414823414554, 0.459292588292723, 0.459292588292723) (0.459292588292723, 0.081414823414554, 0.459292588292723) (0.459292588292723, 0.459292588292723, 0.081414823414554) (0.658861384496480, 0.170569307751760, 0.170569307751760) (0.170569307751760, 0.658861384496480, 0.170569307751760) (0.170569307751760, 0.170569307751760, 0.658861384496480) (0.898905543365938, 0.050547228317031, 0.050547228317031) (0.050547228317031, 0.898905543365938, 0.050547228317031) (0.050547228317031, 0.050547228317031, 0.898905543365938) (0.008394777409958, 0.263112829634638, 0.728492392955404) (0.008394777409958, 0.728492392955404, 0.263112829634638) (0.263112829634638, 0.008394777409958, 0.728492392955404) (0.728492392955404, 0.008394777409958, 0.263112829634638) (0.263112829634638, 0.728492392955404, 0.008394777409958) (0.008394777409958, 0.263112829634638, 0.728492392955404)	0.144315607677787 0.095091634267285 0.095091634267285 0.095091634267285 0.103217370534718 0.103217370534718 0.103217370534718 0.032458497623198 0.032458497623198 0.032458497623198 0.027230314174435 0.027230314174435 0.027230314174435 0.027230314174435
9	(0.333333333333333, 0.333333333333333, 0.333333333333334) (0.020634961602525, 0.489682519198738, 0.489682519198737) (0.489682519198738, 0.020634961602525, 0.489682519198737) (0.489682519198738, 0.489682519198738, 0.020634961602524) (0.125820817014127, 0.437089591492937, 0.437089591492936) (0.437089591492937, 0.125820817014127, 0.437089591492936) (0.437089591492937, 0.437089591492937, 0.125820817014126) (0.623592928761935, 0.188203535619033, 0.188203535619032) (0.188203535619033, 0.623592928761935, 0.188203535619032) (0.188203535619033, 0.188203535619033, 0.623592928761934) (0.0910540973211095, 0.044729513394453, 0.044729513394452) (0.044729513394453, 0.0910540973211095, 0.044729513394452) (0.044729513394453, 0.044729513394453, 0.910540973211094) (0.036838412054736, 0.221962989160766, 0.741198598784498) (0.036838412054736, 0.741198598784498, 0.221962989160766) (0.221962989160766, 0.036838412054736, 0.741198598784498) (0.741198598784498, 0.036838412054736, 0.221962989160766) (0.221962989160766, 0.741198598784498, 0.036838412054736) (0.036838412054736, 0.221962989160766, 0.741198598784498)	0.097135796282799 0.031334700227139 0.031334700227139 0.031334700227139 0.077827541004740 0.077827541004740 0.077827541004740 0.079647738927210 0.079647738927210 0.079647738927210 0.025577675658698 0.025577675658698 0.025577675658698 0.043283539377289 0.043283539377289 0.043283539377289 0.043283539377289 0.043283539377289

References

1. Auricchio, F., Boffi, D., Gastaldi, L., Lefieux, A., Reali, A.: On a fictitious domain method with distributed Lagrange multiplier for interface problems. *Applied Numerical Mathematics* **95**, 36–50 (2015)
2. Boffi, D., Gastaldi, L., Ruggeri, M.: Mixed formulation for interface problems with distributed lagrange multiplier. *Computers & Mathematics with Applications* **68**, 2151–2166 (2014)
3. Brezzi, F.: On the existence, uniqueness and approximation of saddle point problems arising from Lagrangian multipliers. *RAIRO Analyse Numerique* **8**, 129–151 (1974)
4. Brezzi, F., Fortin, M.: *Mixed and hybrid finite element methods*. Springer-Verlag, New York (1991)
5. Chakrabarti, S.K. (ed.): *Numerical Models in Fluid Structure Interaction, Advances in Fluid Mechanics*, vol. 42. WIT Press (2005)
6. Dunavant, D.A.: High degree efficient symmetrical gaussian quadrature rules for the triangle. *International Journal for Numerical Methods in Engineering* **21**(6), 1129–1148 (2010)
7. Glowinski, R., Pan, T.W., Hesla, T., Joseph, D.: A distributed Lagrange multiplier/fictitious domain method for particulate flows. *Int. J. Multiphase Flow* **25**, 755–794 (1999)
8. Hirt, C., Amsden, A., Cook, J.: An arbitrary Lagrangian-Eulerian computing method for all flow speeds. *J. Comput. Phys.* **14**, 227–253 (1974)
9. Hu, H.: Direct simulation of flows of solid-liquid mixtures. *Int. J. Multiphase Flow* **22**, 335–352 (1996)
10. LeVeque, R., Li, Z.: The immersed interface method for elliptic equations with discontinuous coefficients and singular sources. *SIAM J. Numer. Anal.* **31**, 1019–1044 (1994)
11. Li, Z., Lai, M.C.: The immersed interface method for the Navier-Stokes equations with singular forces. *J. Comput. Phys.* **171**, 822–842 (2001)
12. Liu, W.K., Kim, D.W., Tang, S.: Mathematical foundations of the immersed finite element method. *Comput. Mech.* **39**, 211–222 (2006)
13. Lundberg, A., Sun, P., Wang, C.: Distributed Lagrange multiplier-fictitious domain finite element method for Stokes interface problems. *International Journal of Numerical Analysis & Modeling* (submitted) (2018)
14. Peskin, C.: The immersed boundary method. *Acta Numer.* **11**, 479–517 (2002)
15. Sun, P.: Fictitious domain finite element method for Stokes/elliptic interface problems with jump coefficients. *Journal of Computational and Applied Mathematics* **356**, 81–97 (2019)
16. Sun, P., Wang, C.: Fictitious domain finite element method for Stokes/parabolic interface problems with jump coefficients. *Applied Numerical Mathematics* (submitted) (2018)
17. Takizawa, K., Henicke, B., Tezduyar, T.E., Hsu, M.C., Bazilevs, Y.: Stabilized space-time computation of wind-turbine rotor aerodynamics. *Computational Mechanics* **48**, 333–344 (2011)
18. Wang, C., Sun, P.: A fictitious domain method with distributed Lagrange multiplier for parabolic problems with moving interfaces. *Journal of Scientific Computing* **70**, 686–716 (2017)